On the Feasibility of Using Low-Melting Bath to Accommodate Inert Anodes in Aluminium Electrolysis Cells

Asbjørn Solheim

SINTEF Industry, P.O. Box 4760 Torgarden, NO-7465 Trondheim, Norway
e-mail: asbjorn.solheim@sintef.no

Key words: Inert anodes, Low-melting bath, Decomposition, Alumina dissolution

Abstract

Inert anodes for aluminium production can be made of ceramics, metals, or a mixture of those (cermets). Regardless of the type of anode, the surface will be an oxide. With high enough anode potential, the surface oxide will be decomposed upon formation of the corresponding fluoride, eventually leading to a catastrophic defect. The reversible voltage for decomposition was calculated for anode materials based on Ni, Fe, Cu, Co, and Cr in terms of the activities of alumina and aluminium fluoride at 960 °C and at 800 °C. Cu is the most promising candidate, when based on the decomposition voltage alone. It was found that the risk of failure was higher at low temperature, partly because low-melting baths have high activity of aluminium fluoride, and partly because it will be challenging to maintain high enough activity of alumina, even in a "slurry cell" where the bath consists of a suspension of tiny alumina particles. Based on a simplified model for the conditions inside the diffusion layer at the anode, it was estimated that the alumina particles in the slurry cannot be larger than 5-10 microns.

Introduction

Although inert anodes for primary aluminium production was mentioned already in C.M. Hall's basic patent 135 years ago [1], this technology is often presented as new and revolutionary. Currently, inert anodes are pursued in China, in Russia (RUSAL), in Canada and USA (the ELYSIS consortium [2]), and there is also a group in Iceland working with inert anodes (Arctus Metals, [3]).

There are many candidate materials for use as an inert anode. They are normally categorized as ceramics, metals, and composites of ceramics and metals (cermets). As far as it can be determined from the open literature, most research groups are currently working with cermets or metal anodes based on the elements Ni, Fe, and Cu. All these metals produce oxides when exposed to pure oxygen. The working surface properties, and thereby the electrochemical behaviour and rate of corrosion, depend, in principle, only on the surface oxide – regardless of the nature of the bulk anode material. The centre of interest in the present paper is the thermodynamic stability of this surface. Other factors determining a material's suitability as an anode, such as mechanical integrity, electrical conductivity, avoidance of spalling, self-repairing ability, and problem-free connections are of course important, but only if the anode surface is stable.

The electrolyte (bath) in the aluminium electrolysis is based on cryolite. It was originally chosen due to its ability to dissolve aluminium oxide. Unfortunately, cryolite dissolves all oxides, which is the main reason for the lack of success in developing inert anodes. The oxide solubility leads to corrosion of the anode, and the dissolved oxides end up as metallic contaminations in the produced aluminium, rendering it useless for many purposes. An anode wear rate of 10 mm/year entails about 1000 ppm contamination in the produced metal. It is well known that the oxide solubility in cryolitic melts increases with increasing temperature, and it may also be advantageous to have a low NaF/AlF_3 ratio [4]. Lowering the temperature by using a more acid bath is, therefore, the obvious solution to anode corrosion.

The alumina solubility in an acid bath based on Na_3AlF_6-AlF_3-5 wt% CaF_2 at 800 °C will be only about 3 wt% [5]. The electrical conductivity will also be low, about 140 Sm^{-1} [6], which is only 65 percent of the value for a standard Hall-Héroult bath. Currently, the trend seems to be using KF to increase the alumina solubility, but this further reduces the conductivity [7]. The conductivity can be improved by adding LiF, but this will again reduce the alumina solubility. In the following, it will be assumed that the NaF/AlF_3 molar ratio (r) is about 1.4 and that the alumina solubility is about 3 wt% at 800 °C.

The present work addresses a potential showstopper that, in the author's opinion, has not received sufficient attention: When the anode potential is higher than the reversible potential for decomposition of the surface oxide by forming the corresponding fluoride and oxygen, the anode will undergo decomposition or "catastrophic corrosion" [8]. Low alumina activity and high overvoltage increase the anode potential, while high aluminium fluoride activity decreases the potential for surface oxide decomposition. The hypothesis is that the risk of decomposition is higher at low temperature, due to the higher activity of aluminium fluoride in low-melting baths.

Main Reaction and Decomposition Reactions

The main (wanted) anode reaction is the production of oxygen from alumina contained in the electrolyte. At certain conditions, the anode may undergo reactions where oxygen is evolved from the anode surface oxide. There is no principal difference between ceramic anodes, cermets, and metal anodes, since the anode surface consists of oxides in all cases. Decomposition of the anode starts when the anode potential – which is the sum of the reversible potential and the anodic overvoltage for the main reaction – surpasses the reversible voltage for the decomposition reaction in question. It is, therefore, essential to know the potential difference between the main reaction and the destructive reaction in which the anode is consumed. The reversible voltages for all reactions discussed in the following were calculated with thermochemical data taken from Knacke et al. [9].

Activities of Alumina and Aluminium Fluoride

As already mentioned, the reversible voltages for the reactions depend on the activity of aluminium fluoride. The activity of alumina is also of importance, if the surface oxide is an aluminate. The activities of AlF_3 and Al_2O_3 in the system $NaF\text{-}AlF_3\text{-}Al_2O_3$ were derived by Solheim and Sterten [10]. Even though the activities will be influenced by additional substances such as CaF_2, KF, and LiF, which will be present in industrial baths for low temperature applications; the data shown in Figure 1 can serve as a rough guide when discussing the effects of temperature and bath composition. The following should be kept in mind:

- An acidic, lower temperature bath drives a stronger change in alumina activity per mass unit change in alumina concentration.
- An acidic, lower temperature bath (e.g., r = 1.4 at 800 °C) drives a strong increase in the activity of AlF_3. The AlF_3 activity in a standard Hall-Héroult bath is about $3 \cdot 10^{-3}$, ($r \approx 2.3$) while it will be about 0.1 in a low-melting bath.

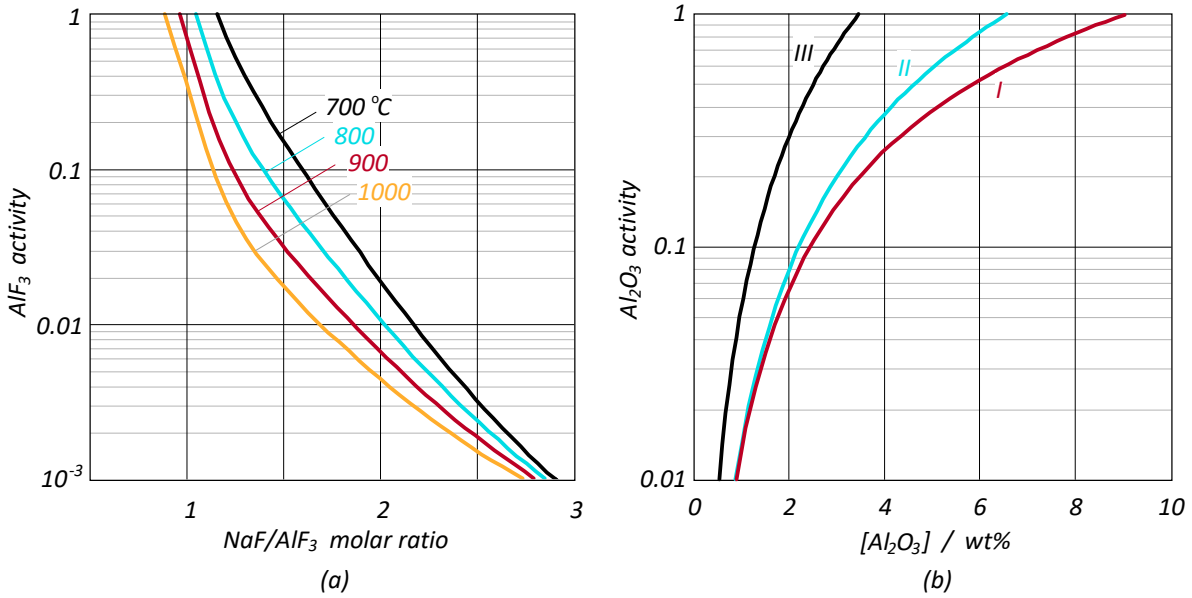

Figure 1. a): Activity of AlF_3 in the system $NaF\text{-}AlF_3$ as a function of the NaF/AlF_3 molar ratio (r) at different temperatures [10]. b): Activity of alumina in the system $NaF\text{-}AlF_3\text{-}Al_2O_3$ as a function of the alumina concentration. I: r = 2.2, 960 °C; II: r = 1.4, 960 °C; III: r = 1.4, 800 °C. The data are partly extrapolated below the liquidus temperature. The standard states are solid AlF_3, liquid NaF, and solid $\alpha\text{-}Al_2O_3$.

Main Reaction

The electrode reactions and the overall reaction in a cell with inert anodes are:

$$Cathode\ reaction\text{:}\ AlF_3(diss) + 3Na^+ + 3e^- \rightarrow Al(l) + 3NaF(l) \quad (1)$$

$$Anode\ reaction\text{:}\quad \tfrac{1}{2}Al_2O_3(diss) + 3NaF(l) \rightarrow \tfrac{3}{4}O_2(g) + AlF_3(diss) + 3Na^+ + 3e^- \quad (2)$$

$$Cell\ reaction\text{:}\quad \tfrac{1}{2}Al_2O_3(diss) \rightarrow Al(l) + \tfrac{3}{4}O_2(g) \quad (3)$$

Provided unit activity for the products, the reversible voltage for the cell reaction is:

$$E_3^{rev} = -\frac{\Delta G_3^0}{3F} - \frac{RT}{3F} ln\left(\frac{1}{a_{Al_2O_3}^{\frac{1}{2}}}\right) \quad (4)$$

where ΔG^0 is the change in standard Gibbs energy, F is Faraday's constant, R is the universal gas constant, T is absolute temperature, and a is activity.

Anodes Based on Nickel

The stable surface component on an inert anode made of nickel or nickel ferrite ($NiFe_2O_4$) will be nickel aluminate ($NiAl_2O_4$) at high alumina concentration and NiO at low alumina concentration. Fe_2O_3 has higher solubility in the bath than the nickel compounds [4] and iron will also disappear into the gas as explained below, leaving the nickel compounds behind. The decomposition reactions are:

$$\tfrac{3}{2}NiO(s) + 3NaF(l) \rightarrow \tfrac{3}{2}NiF_2(s) + \tfrac{3}{4}O_2(g) + 3Na^+ + 3e^- \quad (5)$$

$$\tfrac{3}{2}NiAl_2O_4(s) + 3NaF(l) \rightarrow \tfrac{3}{2}NiF_2(s) + \tfrac{3}{4}O_2(g) + \tfrac{3}{2}Al_2O_3(diss) + 3Na^+ + 3e^- \quad (6)$$

When combined with the cathode reaction (Equation 1, which is common for all cell reactions), the overall decomposition reactions become:

$$\tfrac{3}{2}NiO(s) + AlF_3(diss) \rightarrow Al(l) + \tfrac{3}{4}O_2(g) + \tfrac{3}{2}NiF_2(s) \quad (7)$$

$$\tfrac{3}{2}NiAl_2O_4(s) + AlF_3(diss) \rightarrow Al(l) + \tfrac{3}{4}O_2(g) + \tfrac{3}{2}NiF_2(s) + \tfrac{3}{2}Al_2O_3(diss) \quad (8)$$

With unit activities for all substances except Al_2O_3 and AlF_3, the corresponding reversible voltages are:

$$E_7^{rev} = -\frac{\Delta G_7^0}{3F} - \frac{RT}{3F} ln\left(\frac{1}{a_{AlF_3}}\right) \quad (9)$$

and

$$E_8^{rev} = -\frac{\Delta G_8^0}{3F} - \frac{RT}{3F} ln\left(\frac{a_{Al_2O_3}^{3/2}}{a_{AlF_3}}\right) \quad (10)$$

The reversible voltages for reactions 3, 7, and 8 are compared in Figure 2. The following can be read from the graphs:

- The difference in reversible voltage between the main reaction and the decomposition reactions increase with increasing alumina activity and decreasing activity of aluminium fluoride.
- The difference between the voltages, compared at the same activities, is almost independent of the temperature.
- There is a cell voltage penalty of about 90 mV when reducing the temperature from 960 °C to 800 °C.

Since an acid bath (r = 1.4) working at 800 °C has much higher activity of aluminium fluoride than a standard Hall-Héroult bath (r = 2.3, Figure 1), the voltage difference between the wanted reaction and the decomposition reactions will be smaller at low temperature.

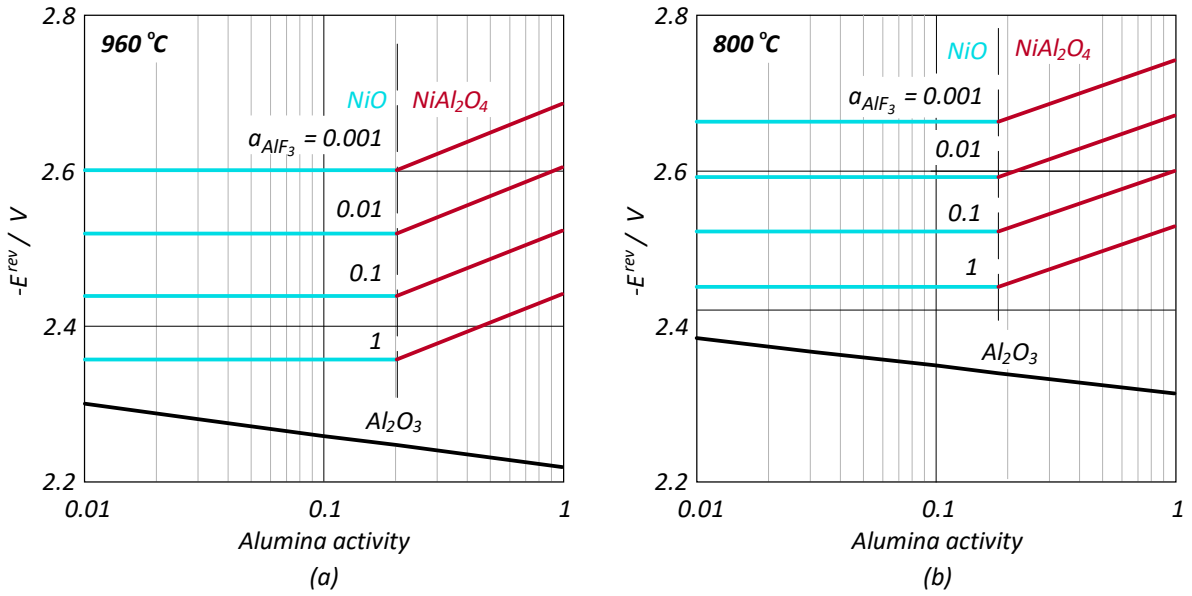

Figure 2. Reversible voltage for oxygen evolution from Al_2O_3, NiO, and $NiAl_2O_4$ (Eqs. 3, 7, and 8) as a function of the alumina activity. a): at 960 °C, b): at 800 °C.

Anodes Based on Iron

With anodes based on iron, Fe_2O_3 will be the stable surface compound in the presence of oxygen. The decomposition reaction is:

$$\frac{1}{2}Fe_2O_3(s) + AlF_3(diss) \rightarrow Al(l) + \frac{3}{4}O_2(g) + FeF_3(s) \quad (11)$$

The reversible voltage is very similar to the corresponding reaction for NiO (Equation 7). Iron aluminate ($FeAl_2O_4$) will not be formed under the actual conditions, however. This entails that the potential difference between the wanted reaction and the decomposition reaction close to alumina saturation is lower than for a nickel-based anode. An additional complication with the iron anode is the high vapour pressure of FeF_3. The vapour pressure can be calculated from the equilibrium:

$$\frac{1}{2}Fe_2O_3(s) + AlF_3(diss) = \frac{1}{2}Al_2O_3(diss) + FeF_3(g) \quad (12)$$

The FeF_3 pressure is proportional with the AlF_3 activity and inversely proportional with the square root of the Al_2O_3 activity. The maximum acceptable pressure, provided that the surface of the anode should not corrode more than 10 mm/year, is $8 \cdot 10^{-4}$ atm (current density: 10 kAm^{-2}, density of Fe_2O_3: 5200 kgm^{-2}). The data in Figure 3 illustrate that this criterion barely can be met at 960 °C, even at alumina saturation (AlF_3 activity $\approx 3 \cdot 10^{-3}$). It will also be difficult to achieve low enough pressure at 800 °C, where the AlF_3 activity will be in the order of 0.1. The evaporated iron ends up in the metal after a short trip through the dry scrubber. The dotted line in Figure 3 corresponds to 0.12 wt% Fe transferred to the produced metal.

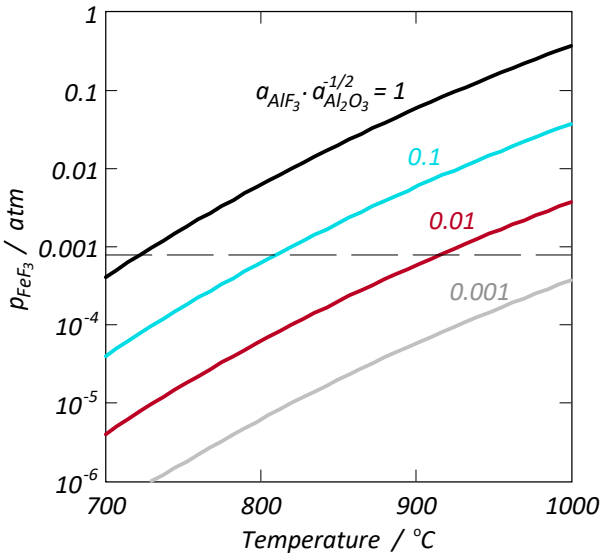

Figure 3. Equilibrium vapour pressure of FeF_3 as a function of the temperature at different activities of AlF_3 and Al_2O_3. The dotted line represents the vapour pressure that gives a Fe_2O_3 corrosion rate of 10 mm/year ($8 \cdot 10^{-4}$ atm).

Anodes Based on Copper

Copper anodes develop a layer of CuO on the active surface at low alumina activity, and $CuAl_2O_4$ is only stable at very high alumina activity. The reversible voltage *vs.* activity diagram resembles the diagram for nickel compounds, see Figure 4. The main difference is that the voltage for consumption of CuO (analogous to Equation 7) is more separated from the voltage for the main cell reaction, making copper anodes safer than nickel anodes at low alumina activity. CuF_2 is liquid at 960 °C and solid at 800 °C.

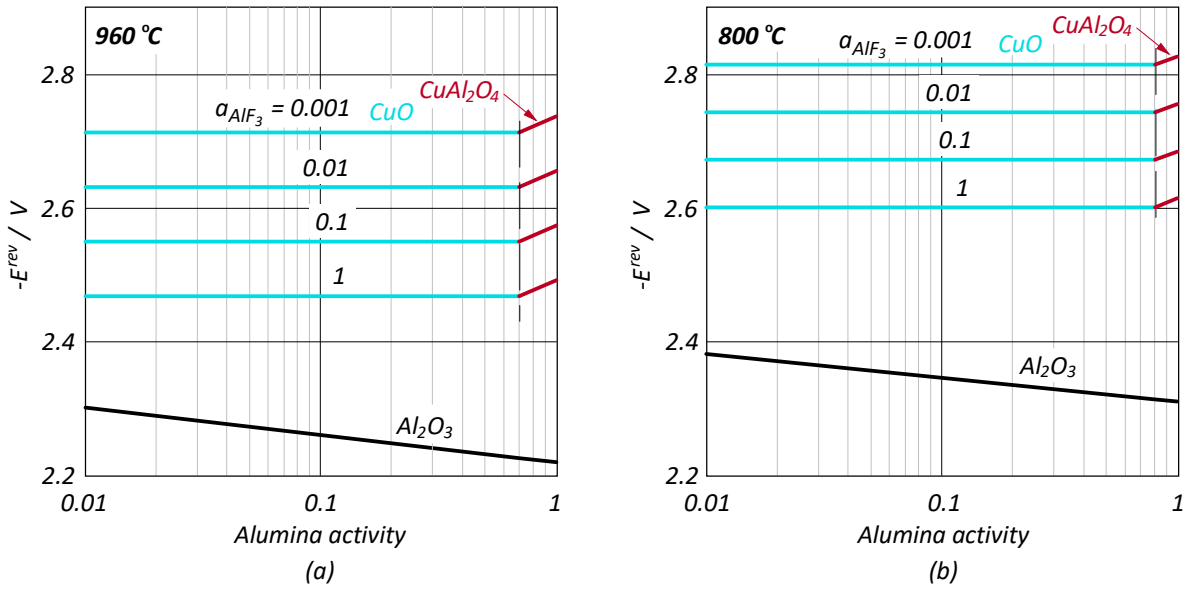

Figure 4. Reversible voltages for oxygen evolution from Al_2O_3, CuO, and $CuAl_2O_4$ as a function of the alumina activity. a): at 960 °C, b): at 800 °C.

Anodes Based on Cobalt or Chrome

The potentials for consumption of cobalt-based anodes resemble the course for nickel. Figure 5 a) illustrates that CoO has a relatively low decomposition potential, and $CoAl_2O_4$ is the stable surface component down to a low alumina activity. Consequently, anodes based on cobalt may work well near alumina saturation, but they are particularly dependent on seeing a high alumina activity.

Chrome oxide (Cr_2O_3) appears to be relatively stable, as shown in Figure 5 b). There is no formation of chrome aluminate.

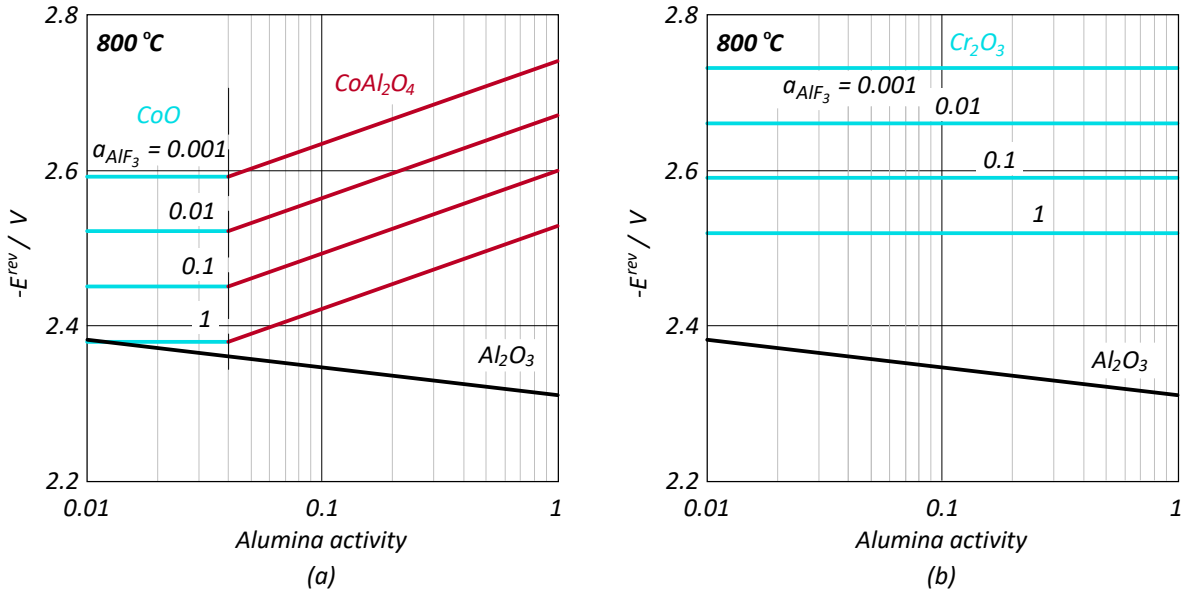

Figure 5. a): Reversible voltages at 800 °C as a function of the alumina activity. a): Oxygen evolution from Al_2O_3, CoO, and $CoAl_2O_4$, b): Oxygen evolution from Al_2O_3 and Cr_2O_3.

Anodic Overvoltage

The maximum anodic overvoltage to avoid decomposition is given by the voltage difference between the alumina curve and the other curves in the preceding figures. The voltage "window" between normal electrolysis and anode decomposition is relatively small, as illustrated in Figure 6. The value of the anodic overvoltage is, therefore, extremely important for the performance of the inert anode. Still, the literature is surprisingly scarce in this field. The overvoltage is often assumed to be 0.1 V, and some studies have indicated overvoltage of that magnitude; e.g., McLeod et al. [11] found that the overvoltage at cobalt ferrite at 10 kAm^{-2} and 960 °C was 0.14 V. However, higher values have also been reported. Du et al. [12] measured 0.31 V on nickel ferrite at 10 kAm^{-2} and 980 °C. The overvoltage must be assumed to be higher at low temperature, and Thonstad et al. [13] measured 0.41 V at 750 °C and 10 kAm^{-2} on a Cu-Ni-Fe alloy.

It follows from Figure 6 that none of the elements can be used if the latter overvoltage value is representative. The picture is more positive at 960 °C. The activity of AlF_3 will be almost two orders of magnitude lower in a standard bath, lifting all curves in Figure 6 by 0.13-0.19 V. DOE's Inert Anode Roadmap from 1998 [14] indicated 0.5 V as the upper limit for overvoltage, but this number appears to be motivated by economy rather than technical feasibility. Based on the risk of oxide decomposition alone, Cu appears to be the most promising candidate.

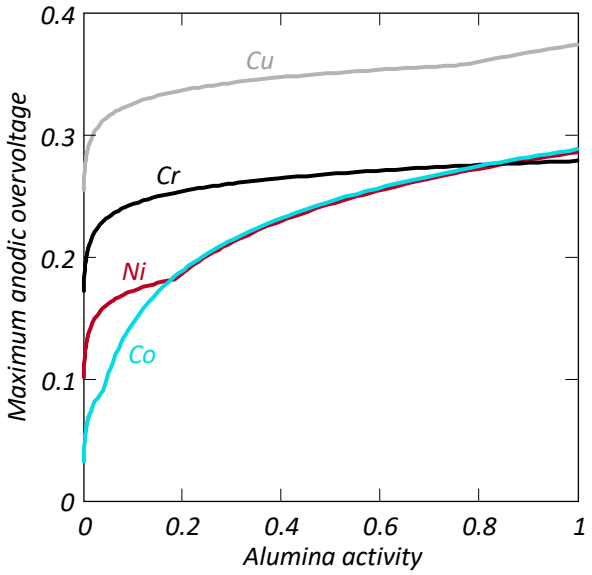

Figure 6. Maximum anodic overvoltage to avoid decomposition as a function of the alumina activity at 800 °C, calculated with an aluminium fluoride activity of 0.1 and anodes based on copper, chrome, nickel, and cobalt.

Alumina Dissolution

Alumina dissolution is mass transfer controlled, which means that the rate of dissolution is proportional with the concentration difference between the alumina surface and the bulk of the bath. The solubility (concentration at the alumina surface) is 8.0-8.5 wt% for a normal Hall-Héroult bath, and the bulk concentration is typically 2-3 wt%. This gives a "driving force" for dissolution of 5-6 wt% alumina. With low-melting baths, the alumina solubility may be as low as 2-3 wt% even with additions of KF – at least if LiF is added to increase the conductivity. The "driving force" should probably not exceed 0.5 wt%. The subsequent discussion is limited to the dissolution of small dispersed alumina particles, pretending that the problem of avoiding agglomeration during feeding has been resolved.

Dissolution of Alumina Particles in the Bulk of the Bath

The diffusion coefficient for alumina in cryolitic melts, based on data from several authors, was suggested to be [15]:

$$D \approx 2.45 \cdot 10^{-6} \cdot exp\left(\frac{-79\,485}{RT}\right) \quad [m^2 s^{-1}] \tag{13}$$

The relatively high activation energy gives a strong temperature dependence, so the diffusion coefficient at 800 °C will be only 31 percent of the value at 960 °C.

The mass transfer coefficient at a sphere can be calculated by the following equation [16],

$$Sh = 2 + 0.6\, Re^{1/2}\, S\, c^{1/3} \tag{14}$$

where Sh, Re, and Sc are the dimensionless Sherwood, Reynold, and Schmidt numbers, respectively. If the particles are small enough (very low Re), the last term in Equation 14 disappears. In the present context, this can be regarded as an acceptable approximation for alumina particles smaller than about 50 µm. With Sh = 2, the time for dissolution (t_{diss}) can be solved analytically [17]:

$$t_{diss} = \frac{d_0^2 \rho_p}{8D \cdot \Delta w \cdot \rho} \tag{15}$$

where d_0 is the original particle diameter, ρ_p is the particle density in air (product of theoretical alumina density and porosity), D is the diffusion coefficient for alumina, Δw is the weight fraction difference between alumina saturation and the bulk concentration, and ρ is the bath density.

If the "driving force" for alumina dissolution is 0.5 wt% Al_2O_3 with inert anodes and 5-6 wt% in a Hall-Héroult cell, the rate of alumina dissolution at 800 °C slows down by a factor of at least 30 compared with the normal Hall-Héroult situation. By taking $\rho_p = 2000$ kgm^{-3} (alumina with 50 vol% pores), $\rho = 2100$ kgm^{-3}, $D = 3.3 \cdot 10^{-10}$ m^{2}s^{-1} at 800 °C, and $\Delta w = 0.005$ (0.5 wt%), the time for dissolution of a 50 µm particle becomes 3 min, while a 30 µm particle dissolves during 1 min.

Perhaps more interesting is the amount of alumina particles that must be kept in suspension to give a dissolution rate corresponding to the electrochemical consumption. It was calculated [18] that a few hundred grams of alumina particles kept in suspension is sufficient to feed a 300 kA Hall-Héroult cell. Using the same treatment for the inert anode cell, the amount of dispersed alumina in an inert anode cell with 0.5 wt% driving force for alumina dissolution becomes 1.2 kg/100 kA for 50 µm particles and 0.4 kg/100 kA with 30 µm particles. The fraction of solid particles in the bath will then be in the order of 0.1 vol%. Intuitively, dissolution of alumina in the bulk of the bath should not be a major problem, provided that agglomeration can be avoided.

Alumina Consumption at the Anode

The dissolved alumina is transported from the bulk to the anode surface by ordinary mass transfer. An equation for the mass transfer coefficient at a gas-evolving electrode was derived by Vogt and Stefan [19].

$$k = 1.65 \cdot \theta^{0.5}(1-\theta) \cdot \left(\frac{GD}{d}\right)^{0.5} \qquad (16)$$

where θ is the gas bubble coverage, G is the rate of gas evolution [m^{3}s^{-1}m^{-2}], and d is the bubble diameter. An equation for the gas bubble coverage was suggested by Vogt and Balzer [20] and modified by Solheim [21]. Mass transfer at a gas evolving surface is relatively rapid since turbulence is generated directly at the surface.

The mass transfer coefficient was calculated as a function of the current density at 95 percent current efficiency and 800 °C. The resulting alumina concentration difference between the bulk of the bath and the anode is shown in Figure 7. Although it is possible that the mass transfer coefficient is somewhat higher than indicated by Equation 16 due to linear flow along the anode, the data in Figure 7 indicate that it is improbable that the alumina concentration at the anode can be kept close enough to saturation in a situation where the solubility is in the order of 3 wt%, unless the cell is operated at very low current density. The only option appears to be the "slurry cell", where solid alumina particles are brought directly to the anode surface.

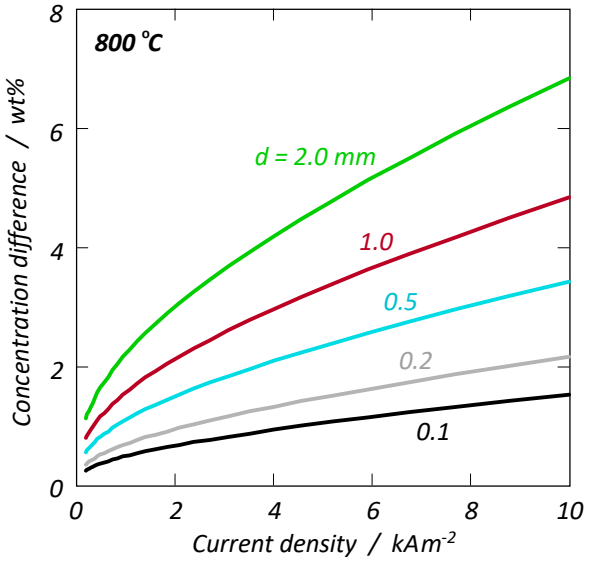

Figure 7. Concentration difference between the bulk of the bath and the anode at 800 °C as a function of the current density with different gas bubble diameters (d).

Slurry Cell

In the slurry cell patented by Beck [22], alumina is transported to the anode in the form of solid particles instead of being transferred in solution. Effectively, this is a way of "shortcutting" the mass transfer limitations, by allowing the alumina to dissolve within the mass transfer boundary layer. Still, the particles will have to dissolve by spherical diffusion (Sh = 2). A rough calculation of the necessary amount of solid alumina at 800 °C very close to the anode is outlined below.

The "diffusion layer thickness" (δ) is defined by $\delta = D/k$. At a current density of 2-10 kAm^{-2}, the diffusion layer thickness at the anode is in the range of 6 µm to 28 µm at 800 °C (gas bubble diameters between 0.1 and 2 mm). A normal alumina particle cannot even be fitted inside the diffusion layer, and it was indicated by Beck [22] that the alumina needs to be very fine. By comparing the anodic consumption rate of alumina (10 kA, 95 percent current efficiency) with the rate of dissolution from a particle with given diameter, it is possible to estimate the number of particles that must be inside the diffusion layer, and thereby, the volume fraction of solid alumina. Some results are shown in Figure 8. It was assumed that the volume outside the diffusion layer is saturated in alumina, and that the average driving force for dissolution is 0.25 wt% Al_2O_3 (0.5 wt% difference across the boundary layer).

The result is shown in Figure 8. As can be observed, the alumina particles must indeed be very small, and the volume fraction for particles larger than about 5-10 µm needs to be high to match the anodic consumption of alumina. The particle volume fraction cannot be higher at the anode than in the bulk, so it appears that the entire cell must be operated with a sludge-like suspension of tiny alumina particles.

A similar conclusion, based on an extensive amount of experimental data, was drawn by Yasinskiy et al. [23]. They recommended that a 12 vol% suspension of 5 µm alumina particles should be further studied.

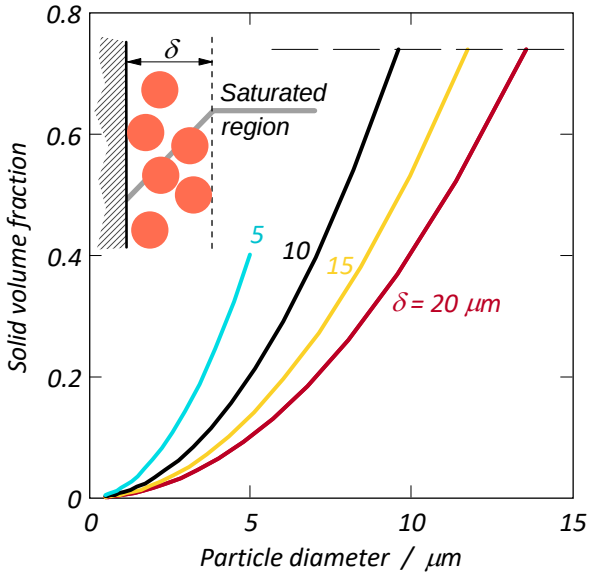

Figure 8. Volume fraction of solid particles inside the diffusion layer as a function of the particle diameter. Parameter: Diffusion layer thickness. The horizontal dotted line indicates the maximum packing density for equal spheres, and the insert illustrates alumina particles inside the diffusion layer.

Concluding Remarks

To the author's knowledge, the increased risk of damaging inert anodes by chemical decomposition at low temperature has not been addressed earlier in the open literature. Much of the research in the field of inert anodes apparently still takes place in the form of laboratory and pilot scale experiments lasting for a few hours, mostly focusing on the development and testing of materials and alloys. Even though there certainly exist significant developments and scientific results that have not been published; more basic research concerning the electrochemistry of inert anodes should be encouraged. A key factor is the anodic overvoltage. Candidate materials should be screened and optimised regarding this parameter, which is particularly important at low temperature.

There are challenges related to alumina quality and alumina feeding. Is it possible to produce and handle the extremely fine-grained alumina required? Is it possible to feed it without agglomeration? Can it be used in a dry scrubber? How will the convection and slurry transport conditions be in a cell operating with small anode-cathode distance? All this will be easier to solve if the cell is operated at low current density, which cannot be considered as an economically viable option.

Many of the estimates in the present paper, particularly the treatment of the alumina dissolution, are rough and made with simplistic assumptions – much like playing a piece of music ignoring all the flats and sharps: The result will be less than fully correct, but perhaps still interesting. Hopefully, the estimates can be verified with more sophisticated theories and computation tools, such as CFD.

Acknowledgement

The present work was supported by the Research Council of Norway and the end-user partners of HighEFF (Centre for an Energy Efficient and Competitive Industry for the Future), which is an eight-year program as a Centre for Environment-friendly Energy Research.

References

1. C. M. Hall: Process of Reducing Aluminium Electrolysis, US Patent No. 400,766 (9 July, 1886).
2. ELYSIS, https://www.elysis.com/
3. G. Gunnarsson, G. Óskarsdóttir, S. Frostason, and J. H. Magnússon: Aluminum Electrolysis with Multiple Vertical Non-consumable Electrodes in a Low Temperature Electrolyte, *Light Metals 2019*, 803-810.
4. T.E. Jentoftsen, O.-A. Lorentsen, E.W. Dewing, G.M. Haarberg, and J. Thonstad: Solubility of Some Transition Metal Oxides in Cryolite-Alumina Melts: Part I. Solubility of FeO, $FeAl_2O_4$, NiO, and $NiAl_2O_4$, *Met. and Mat. Trans. B*, **33B**, 901-908 (2002).
5. E. Skybakmoen, A. Solheim, and Å. Stertendfgjkløæ'
6. qw56789: Alumina Solubility in Molten Salt Systems of Interest for Aluminium Electrolysis and Related Phase Diagram Data, *Met. Trans. B* **28B** 81-86 (1997).
7. D. Uher, L. Cirka, J. Kamenar, and J. Hives: A New Type of Aluminium Smelting Baths Electrical Conductivity, *Acta Chemica Slovaca* **2** (1) 25-30 (2009).
8. A. Redkin, A. Apisarov, A. Dedyukhin, V. Kovrov, Yu. Zaikov, O. Tkacheva, and J. Hryn: Recent Developments in Low-Temperature Electrolysis of Aluminum, *ECS Transactions* **50** (11) 205-213 (2012).
9. H. Xiao, R. Hovland, S. Rolseth, and J. Thonstad: Studies on the Corrosion and the Behavior of Inert Anodes in Aluminum Electrolysis, *Met. and Mat. Trans. B*, **27B** (2) 185-194 (1996).
10. O. Knacke, O. Kubaschewski, and K. Hesselmann (Eds.): Thermochemical Properties of Inorganic Substances, 2nd Ed., Springer-Verlag, 1991.
11. A. Solheim and Å. Sterten: Activity of Alumina in the System NaF-AlF_3-Al_2O_3 at NaF/AlF_3 Molar Ratios Ranging from 1.4 to 3, *Light Metals 1999*, 445-452.
12. A.D. McLeod, J.S. Haggerty, and D.R. Sadoway: Inert Anode Materials for Hall Cells, *Light Metals 1986*, 269-273.
13. J. Du, B. Wang, Y. Liu, G. Yao, Z. Fang, and P. Hu: Study on the Bubble Behavior and Anodic Overvoltage of $NiFe_2O_4$ Ceramic Based Inert Anodes, *Light Metals 2015*, 1193-1197.
14. J. Thonstad, A. Kisza, and J. Hives: Anode Overvoltage on Metallic Inert Anodes in Low-Melting Bath, Light Metals 2005, 373-377.
15. *Inert Anode Roadmap*, Department of Energy (USA), Office of Energy Efficiency and Renewable Energy (1998):
16. A. Solheim and E. Skybakmoen: Mass- and Heat Transfer Phenomena in Dissolution of Alumina, *Light Metals 2020*, 664-671.
17. R.B. Bird, W.E. Stewart, and E.N. Lightfoot, *Transport Phenomena*, p. 333, John Wiley & Sons, Inc., New York, 1960.
18. J. Thonstad, A. Solheim, S. Rolseth, and O. Skar: The Dissolution of Alumina in Cryolite Melts, *Light Metals 1988*, 655-661.
19. A. Solheim: A Novel Design Criterion for Alumina Feeders in Aluminium Electrolysis Cells, *Light Metals 2014*, 711-716.
20. H. Vogt and K. Stephan: Local Microprocesses at Gas-evolving Electrodes and Their Influence on Mass Transfer, *Electrochim. Acta* **155** 348-256 (2015).
21. H. Vogt and R.J. Balzer: The Bubble Coverage of Gas-Evolving Electrodes in Stagnant Electrolytes, *Electrochim. Acta* **50** (10) 2073-2079 (2005).

22. A. Solheim: Entropic Heat Effects in Aluminum Electrolysis Cells with Inert Anodes, *Metall. Mater. Trans. B*, **47** (2) 1274-1279 (2016).
23. T.R. Beck: Electrolytic Reduction of Alumina, United States Patent No. 4 865 701 (1989).
24. A.S. Yasinskiy, S.K. Padamata, P.V. Polyakov, A.S. Samoilo, A.V. Suzdaltsev, and A.Yu. Nikolaev: Electrochemical Behaviour of Cu-Al Oxygen-Evolving Anodes in Low-Temperature Fluoride Melts and Suspensions, *Light Metals 2020*, 591-599.